Precise particle size control during spherical agglomeration of benzoic acid by modification of the bridging liquid phase using TWEEN 20

DOI: 10.1016/j.powtec.2023.119194
Handle: http://hdl.handle.net/1942/49502

Precise Particle Size Control during Spherical Agglomeration of Benzoic Acid by Modification of the Bridging Liquid phase using TWEEN 20.

Nele Merkelbach[a,*], Christos Xiouras[b,*], Arne Vancleef[a], Leen C.J. Thomassen[a], Leen Braeken[a,*]

[a]KU Leuven, Department of Chemical Engineering, Process Engineering for Sustainable Systems, Research unit CIPT, Campuslaan 25, B-3590 Diepenbeek, Belgium

[b] Chemical and Pharmaceutical Development and Supply (CPDS), Janssen R&D, Turnhoutseweg 30, 2340 Beerse, Belgium

*Corresponding author: nele.merkelbach@kuleuven.be, cxiouras@its.jnj.com, leen.braeken@kuleuven.be

The interest in spherical agglomeration processes in the pharmaceutical industry is rising due to the possibility of direct tableting of Active Pharmaceutical Ingredients and enhancements in bulk powder properties translating into improved powder processability. While agglomerating needle-shaped particles into spheres offers numerous advantages, such as improved flowability, filterability, and particle density, achieving precise control over the particle size and shape of the agglomerates remains a significant challenge. More specifically, the obtained agglomerate size rarely reaches values below 500 µm, which is the desired size range for pharmaceutical applications. To address this challenge, the current research investigates the effectiveness of incorporating surfactants at varying concentrations as a means to control the particle size and shape of the resulting agglomerates. Reversed addition antisolvent crystallization experiments were performed in ethanol/water using benzoic acid as a model compound, followed by the addition of a bridging liquid (toluene), which wets and bridges the single crystals into agglomerates. To modify the interfacial tension between the two immiscible liquid phases, different concentrations of the tween 20 surfactant were used, leading to a range of interfacial tensions spanning from 0.50 to 16.38 x 10^{-3} N/m. Both crystallization and agglomeration processes were monitored in situ using in-process microscopy tools. The experimental results demonstrated that by adjusting the surfactant concentration and thus the corresponding interfacial tension of the bridging liquid, highly tunable agglomerate sizes were achieved, ranging from 160 µm to 4412 µm. A higher surfactant concentration is correlated with smaller agglomerates and is key to control the final agglomerate size. However, it should be noted that the introduction of surfactants in the spherical agglomeration process negatively impacted the agglomerate's strength. Nonetheless, this method remains a promising and innovative technique for controlling the final particle size during spherical agglomeration.

Keywords: Spherical agglomeration – Interfacial tension – Benzoic acid – Crystallization

1 Introduction

In the pharmaceutical industry, oral solid dosage forms (e.g. tablets) are the most common drug delivery systems used for small molecule active pharmaceutical compounds (APIs) [1]–[3]. Prior to the manufacture of such oral solid dosage forms, solid API forms are needed, which are commonly obtained through crystallization processes. The aforementioned crystallization processes may often result in needle- or plate-shaped morphologies, which are unfavorable due to their poor flowability, compressibility, and processability [4]–[7]. These micrometric properties have a direct influence on the efficiency of API transportation between the downstream processes, but also on downstream processes such as filtration, tableting, and drying, among others [4], [5], [8]. To address such problematic crystal morphologies, the pharmaceutical industry has been traditionally relying on particle engineering approaches as thermal cycling or wet milling or by precise control of the crystallization process parameters, such as the supersaturation. Costly post processing techniques such as dry milling or wet

granulation are often applied when other techniques fail to deliver the desired morphology and particle size. Despite their effectiveness, these methods often struggle to achieve the desired product attributes.

An alternative and promising particle engineering technique is spherical agglomeration (SA) [9]–[12], in which an immiscible bridging liquid (BL) is added to the crystallization system to trigger the formation of spherical agglomerates with favorable bulk powder properties. The spherical agglomeration process can be implemented right after the crystallization step of the primary (e.g. needle or plate like) particles using the same process equipment, and consists of two distinct steps: the wetting and the growth step. During the wetting step, individual crystals are connected via liquid bridges in order to form loose aggregates [12]–[14]. Subsequently, these initial aggregates grow into more compact spherically agglomerated structures due to the applied shear forces enabled by mixing [5], [15], [16]. An important parameter in the spherical agglomeration process is the interfacial tension of the bridging liquid compared to the crystallization solvent system, as it determines the wetting behavior and the initial BL droplet size [4]. However, the exact mechanism and importance of both parameters and their correlation with final agglomerate size and shape are not yet fully understood.

Table 1 provides an overview of studies investigating the process parameters and bridging liquids for spherical agglomeration of benzoic acid, along with the corresponding agglomerate size ranges achieved. The bridging liquid to solid ratio (BSR) [2], [11], [17], agitation speed [5], [17], solid concentration [17] and temperature [18], [19] are the parameters which have a predominant effect on the size of the spherical agglomerates. Additionally, the choice of the bridging liquid is important, which in general should be immiscible with the crystallization solvent system and should have good wettability for the API [6], [13], [17], [20]. Two wetting mechanisms were distinguished: a) the immersion and b) distribution mechanisms (Figure 1a), based on the single crystal size to BL droplet size ratio [14]. The immersion mechanism occurs when the droplets are larger than the crystals, and vice versa for the distribution mechanism [12]–[14].

Table 1: Overview of studies investigating the spherical agglomeration of benzoic acid: the used method and BL, the varied parameters resulting in agglomerates and the obtained particle sizes.

Reference	Method	Bridging liquid	Parameters	Agglomerate size range (µm)
Thati and Rasmuson [9]	AS → BL → BA solution	Heptane	Bridging liquid	800-1500 (D50)
		Toluene	BSR	500-1100 (D50)
		Chloroform	Temperature	500-1150 (D50)
		Cyclohexane	Residence time	1200-1750 (D50)
		Pentane		
Katta and Rasmuson [11]	AS → BA solution → BL	Chloroform	BSR	400-850 (D50)
			BA concentration	450-1150 (D50)
			Stirring rate	450-850 (D50)
	AS → BA solution + BL	Chloroform	/	Around 1000 (D50)
Pena et al. [10]	AS → BA solution + BL	Toluene	BA concentration	1450-2200 (mean)
			Solution to AS ratio	1450-1800 (mean)
	AS → BA solution → BL	Toluene	BA concentration	550-2200 (mean)
			Solution to AS ratio	600-2200 (mean)
Yu et al. [14]	Varying	Cyclo-hexane	Method	2000-5000 (mean)

Orlewski et al. [5]	AS → BA solution → BL	Toluene	BL feeding pipe dimensions	750-2250 (Mean)
Pena and Nagy [21]	Two stage MSMPR: crystallization	Toluene	BA concentration	Around 500 (peak chord length)
			Solution to AS ratio	
Thati and Rasmuson [16]	AS → BA solution + BL	Toluene	BSR	300-1500 (D50)
			BL feeding rate	1250-1800 (D50)
			Amount of solvent	1500-1800 (D50)
Pena et al. [22]	Oscillatory flow baffled crystallizer	Toluene	Residence time	1400-3000 (mean)
			BSR	2300-3000 (mean)
			Solution to AS ratio	1400-1600 (mean)
			BA concentration	1500-1700 (mean)

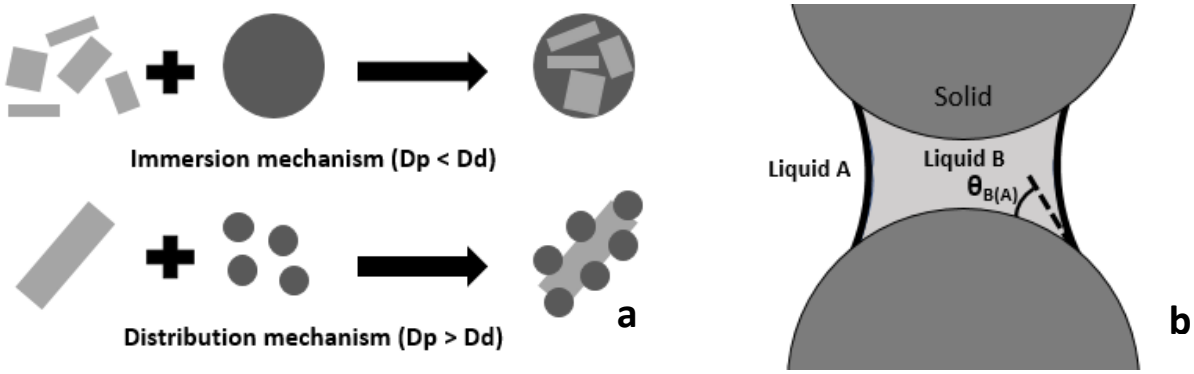

Figure 1: *Different wetting mechanisms determined by the ratio of particle size compared to the droplet size of the BL (a) and the interface of liquid A (solvent) and liquid B (bridging liquid) between two solid particles (b).*

The principle of wetting two particles with the bridging liquid is shown in Figure 1b. The contact angle on the solid surface ($\theta_{B(A)}$) determines the ease of pulling the particles together and is influenced by the wettability and interfacial tension. The interfacial tension seems to play an important role in the wetting behavior of the particles. Previous studies have reported that low interfacial tension results in agglomerates with a low mean size and fracture stress. Furthermore, in some cases, no spherical agglomerates were formed when a BL with a very low interfacial tension was used [4]. On the other hand, a high interfacial tension results in larger droplets and droplets also tend to coalescence more, resulting in even larger droplets. As a result, weaker liquid bridges are formed between the single crystals in the droplet. As shown in Table 1, most of the agglomerates were larger than 1000 µm, which is very large for an active pharmaceutical compound. Therefore, these agglomerates need to be grinded or milled again in further steps. The study of Thati and Rasmuson [16] resulted in the smallest agglomerates of 300 µm. Only for a few experiments, the obtained agglomerates were smaller than 500 µm, which is a more useful size range for the pharmaceutical industry.

The goal of this research is to understand the effect of surfactant addition on the interfacial tension and on the wetting behavior of the bridging liquid during spherical agglomeration and thus on the obtained particle size. The final aim is to reproducibly generate spherical agglomerates with a specific agglomerate size by changing the BL properties. The interfacial tension between the bridging liquid and the crystallization system was adapted by addition of different surfactant concentrations to the bridging liquid phase. Additionally, the effect of surfactant on agglomerate purity and final agglomerate strength was investigated.

2 Materials and methods

2.1 Materials

Benzoic acid (BA) with a purity of 99% was purchased by Alfa Aesar. For the antisolvent crystallization experiments, analytical reagent grade ethanol absolute (≥ 99.8%) was used as the solvent and demineralized water was used as the antisolvent (AS). HPLC grade toluene purchased from Merck was used as the bridging liquid, and different amounts of surfactant were added and dispersed in it. The surfactant used was Tween 20 (also known as Polysorbate 20) purchased by Thermo Scientific.

2.2 Interfacial tension measurements

The interfacial tension between the mixtures of toluene and Tween 20 in water-ethanol was measured by the optical tensiometer Attension theta lite at 22 °C. The cuvette was filled with a water-ethanol mixture in the same volume ratio as during the experiments (425 mL/25 mL). The mixtures of toluene and Tween 20 were loaded into the syringe, which was equipped with a needle. Because the densities of the toluene mixtures were lower than those of the water-ethanol mixture, the needle was bent in such a way that the droplets would come out of the needle pointing upwards. A camera captured images of the outgoing droplets, the contact angle was measured from the image taken just before the droplet emerged from the needle. The interfacial tension was calculated from the measured contact angle by fitting the drop shape with the Young-Laplace equation.

2.3 Bridging liquid droplet size distribution determination

The droplet size of the water-toluene-tween 20 emulsions were characterized in the absence of benzoic acid. The droplet sizes of the different toluene – Tween 20 mixtures were determined inside the 1 L Optimax 1001 Mettler Toledo automated lab reactor without performing the crystallization step. The spherical agglomeration procedure was followed, but instead of adding the solvent mixture of ethanol and benzoic acid, 25 mL of pure ethanol was added at a flow rate of 10 mL/min.

2.4 Spherical agglomeration experiments

All experiments were performed in a 1 L Optimax 1001 (Figure 2) Mettler Toledo automated lab reactor (ALR) equipped with a 45° downward pitched 4-blade turbine impeller for stirring. For the reversed addition antisolvent crystallization, 425 mL demineralized water (used as the antisolvent) at 20 °C was first added into the reactor and stirred at 300 rpm. Subsequently, a Mettler Toledo syringe pump (SP-50 dosing unit) was used to add 25 mL of the benzoic acid solution in ethanol (375 g/L-solvent, constant for all experiments) at room temperature into the reactor at a flow rate of 10 mL/min above the liquid surface. After the benzoic acid solution addition, the reactor was stirred at 300 rpm for 5 min, after which the stirring speed was increased to 1000 rpm in 10 seconds. Next, 7 mL of the bridging liquid, a mixture of toluene and varying amounts of Tween 20 (0.095 - 23.29 g/L), was added at a flow rate of 2 mL/min using a second syringe pump (dosing unit SP-50). The solution of toluene – Tween 20 was constantly stirred with a magnetic stirrer to ensure a homogeneous mixture. After the bridging liquid addition, the reactor was stirred for 5 min to complete the agglomeration process. Subsequently, the formed particles were filtered under vacuum with a Büchner funnel using Whatman blue ribbon 589/3 filter paper. The particles were washed three times by pouring 10 mL demineralized water over the wet cake. Finally, the particles were dried on a petri dish in a vacuum oven at 25 °C for a minimum of one week.

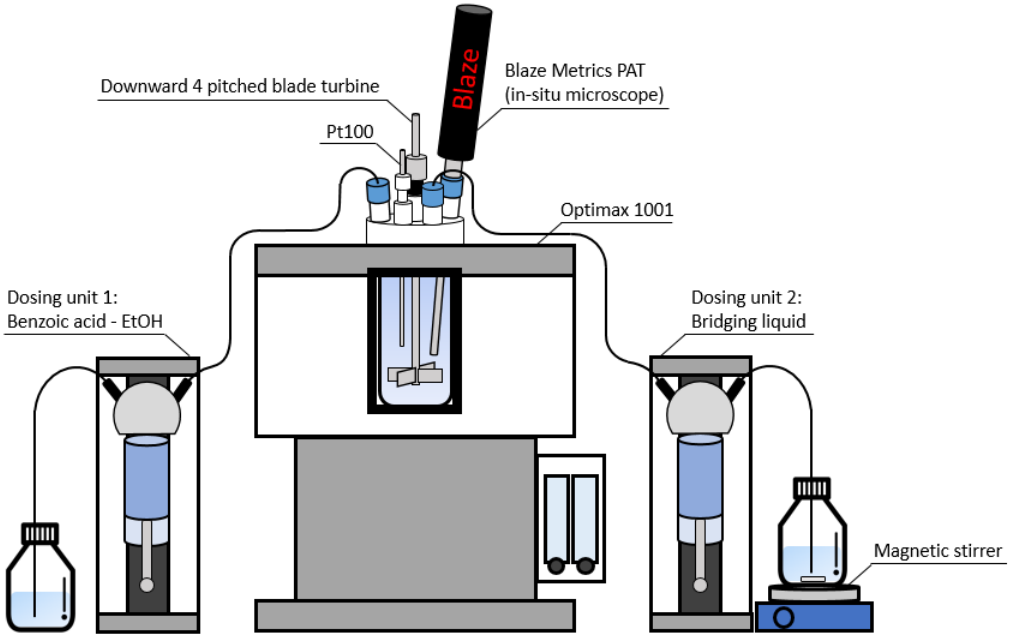

Figure 2: *Experimental set-up: Optimax automated lab reactor with two dosing units for the BL and the solvent.*

2.5 Antisolvent crystallization

The antisolvent crystallization was also performed without the agglomeration step to investigate the influence of the agglomeration step on the formation of the single crystals. 425 mL of water (20 °C) was poured into the reactor and stirred at 300 rpm. Then, 25 mL of the solvent (375 g benzoic acid per L ethanol) was added at 10 mL/min to start the crystallization, followed by a growth step lasting 5 min. The stirring speed was increased to 1000 rpm in 10 seconds, followed by the addition of a single droplet of Tween 20 weighing 46 mg to simulate and obtain the effect of Tween on the crystallization system. The same procedures for filtration, washing and drying were followed.

2.6 Inline particle and droplet analysis

For the inline visualization and analysis of the droplet and particle sizes, the Blaze 900 probe from Blaze Metrics was used (Blaze Metrics process analytical technology). The principle of this tool is Focused Beam Reflectance Measurements (FBRM) to obtain image derived chord length distributions. The probe was immersed inside the reactor, as shown in Figure 2. A 14-bit HDR in-process microscope makes images at a frame rate of 1 frame/second, visualizing the process. The analyzed images provided measurements of chord lengths and particle counts as a function of time.

2.7 Offline particle analysis

Offline particle size analysis was done for the larger agglomerates that were not accurately measured by the Blaze 900 probe. After the drying process, the agglomerates were dispersed over a black background while minimizing overlap. An image of these agglomerates was captured using a standard camera and microscopy and analyzed by the open-source software ImageJ in comparison with an open access algorithm created by Vancleef et al. [23]. Images were obtained using a camera (uEye XS 2, iDS, Obersulm, Germany) and for smaller particles a microscope (Zeiss Primo Star, 40× magnification, Oberkochen, Germany).

2.8 Scanning electron microscope (SEM)

SEM images were captured by the Phenom Pro desktop SEM. The particles were attached and dispersed on a SEM sample stub with a double-sided carbon adhesive pad. These samples were coated with gold using a Quorum Q150R Plus automatic sputter coater.

2.9 GC-FID

The residual toluene content of the formed agglomerates was measured by a GC-FID analysis equipped with a DB-5MS column from Agilent Technologies. A calibration line was constructed between 1.976 and 19.76 mg of toluene per liter of dichloromethane. For every sample, 0.2 g was dissolved in 2 mL of dichloromethane and analyzed by GC-FID. The inlet temperature was 270 °C with a split vent flow rate of 20 mL/min. The sample was injected by a splitless-injector at a flow rate of 1.2 mL/min. The temperature profile in the oven started with a hold at 35 °C for 1 min, afterward the temperature increased at 25 °C/min to reach 270 °C and hold for 0.5 min. The toluene was detected at 270 °C with a 30/400 H_2/air flow ratio.

3 Results and discussion

3.1 Influence of tween 20 on interfacial tension of toluene

The measured interfacial tensions as a function of the tween 20 concentration in toluene are shown in Figure 3a. In general, the interfacial tension decreases with increasing surfactant concentration. In the lowest concentration range between 0.09 g/L and 1.49 g/L, the interfacial tension exhibits a steep drop from 15.56 x 10^{-3} N/m to 3.79 x 10^{-3} N/m. The interfacial tension further decreases and reaches a value between 0.7 and 0.4 x 10^{-3} N/m for the largest concentrations between 7.47 and 55.32 g/L.

During the measurements at the highest concentration (55.32 g/L), some tween 20 was visually extracted from the water phase, as shown in Figure 3b. Therefore, this concentration was not assessed further in the crystallization experiments. Compared to the results of Bak and Podgórska [24] a similar trend was obtained. The absolute values of interfacial tension are different in this study, since tween 20 was dissolved in the toluene phase and a water-ethanol mixture was used, whereas Tween 20 was dissolved in pure water and the organic phase was pure toluene in the research of Bak and Podgórska [24].

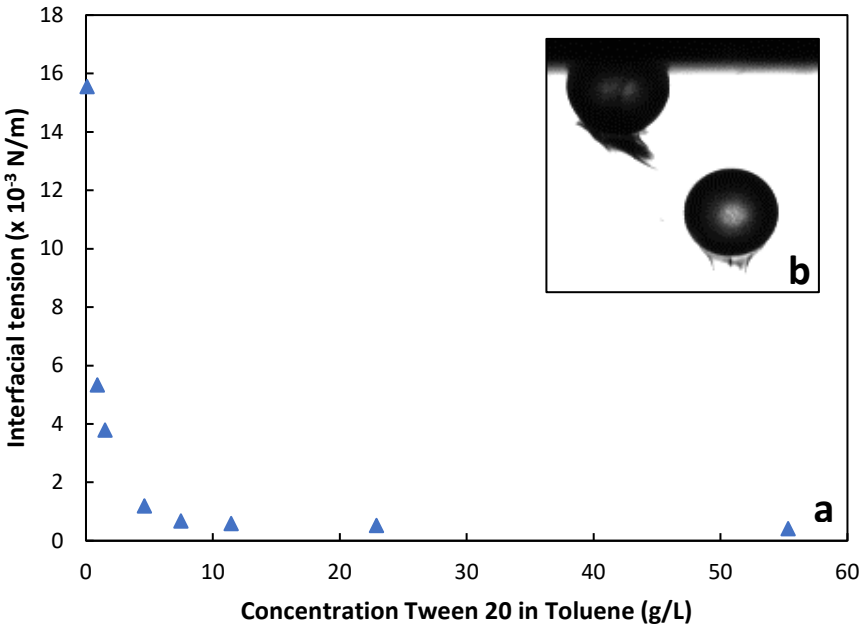

Figure 3: *Interfacial tension measurements of Toluene in a water/ethanol mixture at varying Tween 20 concentrations (a) and an image of the measured droplets at 55.32 g/L (b) at 22 °C.*

3.2 Bridging liquid droplet size

The bridging liquid droplets were analyzed inline to determine the effective droplet sizes and their evolution in time inside the batch reactor. Six toluene – Tween 20 mixtures were added to the crystallization system in the absence of benzoic acid. In Figures 4a-e the mean droplet size (Δ), D10 (X), D50 (○) and D90 (□) of these droplets were plotted against the interfacial tensions at five different times,

i.e., 50, 100, 200, 500 and 1000 seconds after the start of the BL addition. After 50 seconds of addition (Figure 4a), the microscopic Blaze images show only a few droplets, and most of them are even out of focus, due to the low amount of toluene – tween 20 mixture inside the reactor (1.67 mL). These measurements need to be interpreted with caution. Over time, the mean droplet size decreases from approximately 160 µm to 40 µm. The droplet size distribution becomes narrower over time, as shown by the values of D10 and D90 approaching each other. Droplet break-up also occurs faster at lower interfacial tensions, as seen by a steeper decrease at the beginning of the curve between Figures 4a-c. After the completion of the bridging liquid addition (Figure 4 d-e), no significant changes in droplet size were observed, indicating that droplet breakup occurs relatively quickly after addition. In general, the decrease in droplet size occurs faster at lower interfacial tensions, at which the lowest droplet sizes are measured but the final variations in measured droplet sizes are rather limited. For example, after 200 seconds, the mean droplet size ranges from 70 µm to 112 µm for interfacial tensions between 0.50 x 10^{-3} N/m and 16.39 x 10^{-3} N/m.

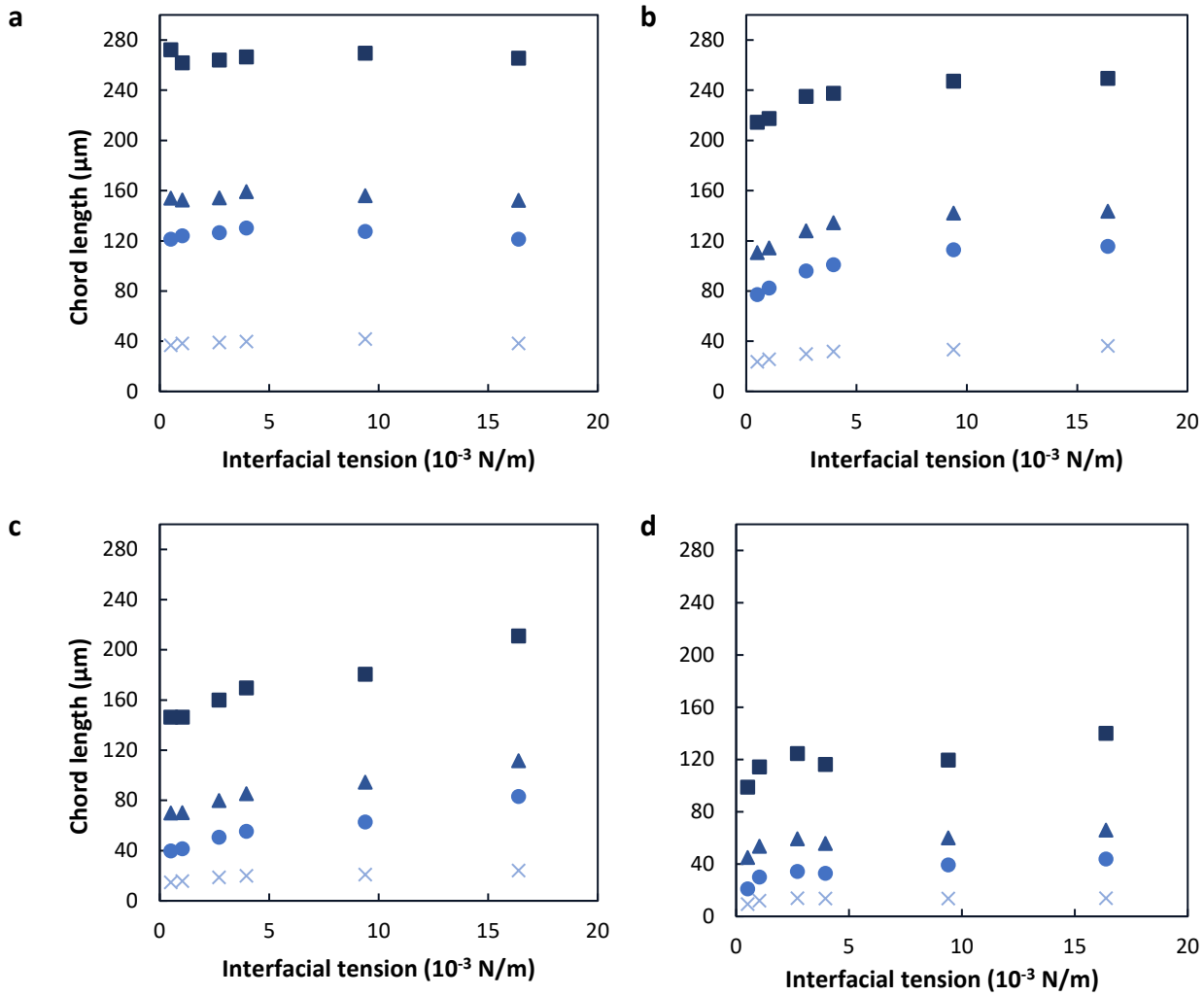

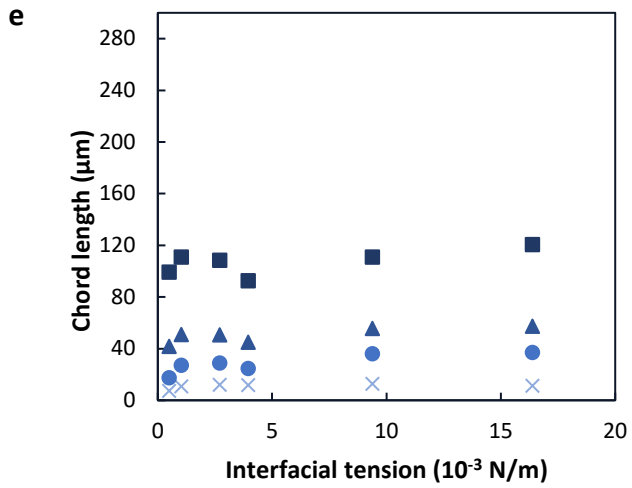

Figure 4: *The mean chord length ▲, D10 **X**, D50 ● and D90 ■ of the toluene droplets against the interfacial tension five different times after the start of BL addition: a) 50s, b) 100s, c) 200s, d) 500s and e) 1000s.*

Figure 5 shows the chord length distributions (CLD) for the droplets after 200 seconds or 6.66 mL of toluene – tween 20 addition for all different mixtures and thus interfacial tensions. The droplet size distribution shows a bimodal graph that appears as a function of time with a first peak between 30 and 40 µm and a second peak around 100 µm. The lower the interfacial tension, the faster the small droplets appear. From figure 5, it can be concluded that the differences in BL droplet size between the different interfacial tensions are rather limited.

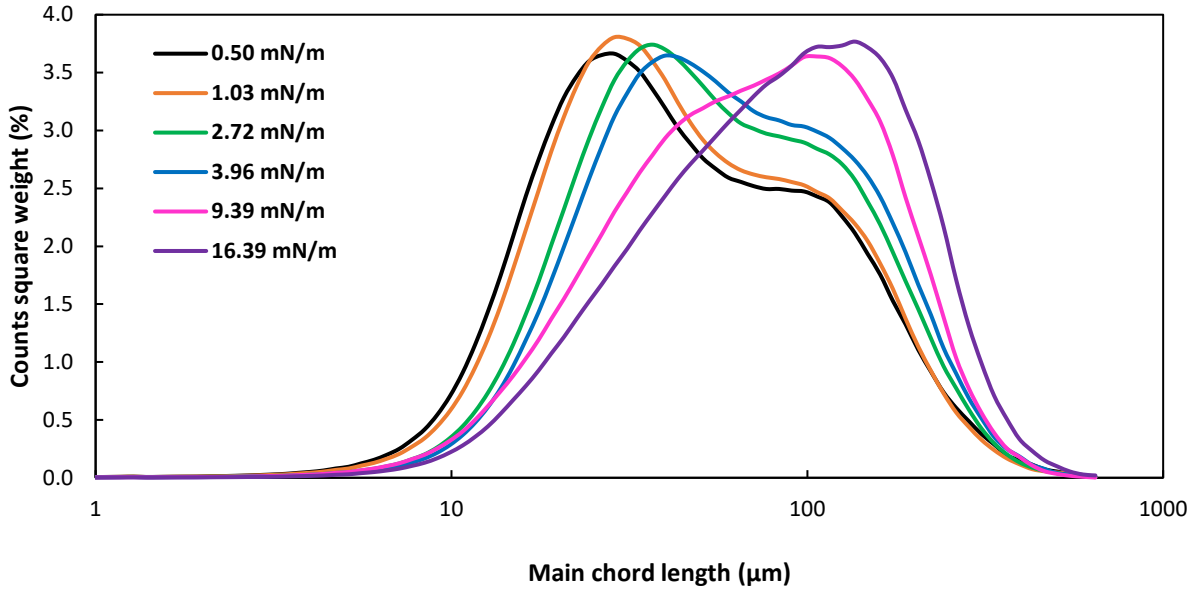

Figure 5: *Chord length distributions of the BL droplets inside the batch reactor after 200s of BL addition for all tested interfacial tensions.*

3.3 Spherical agglomeration

The influence of the interfacial tension between the bridging liquid and the crystallization liquor on spherical agglomerate size and strength was investigated in a spherical agglomeration process of benzoic acid. The same toluene – tween 20 mixtures as in the droplet size investigation were used, but two more intermediate concentrations (11.50 and 4.63 g/L) were added, resulting in interfacial tensions of 0.79 and 1.40 x 10^{-3} N/m, respectively. Figure 6 shows the chord length distributions of the spherical agglomerates obtained by the Blaze Process Analytical technology for interfacial tensions up to 2.72 x 10^{-3} N/m. In the

case of higher interfacial tensions, the resulting agglomerates exceeded 700 µm in size, which exceeded the detection limit of the probe utilized in the experiment. This is visible in Figure 6 by the curve representing 2.72 N/m in which the maximum of the second peak is no longer visible and only the increase in counts to the maximum is shown. Figure 6 also clearly shows a bimodal distribution for all surfactant concentrations, with first a smaller peak around 15-25 µm and then a larger peak that shifts to higher particle sizes with decreasing surfactant concentration. It was assumed that this first peak was caused by the small bridging liquid droplets. Supporting evidence was obtained by comparing the peak position with the bimodal CLD of the droplets (Figure 5), where a similar peak was found at comparable droplet sizes. Figure 6 also shows that this peak of the droplets shifts to slightly higher values, when the interfacial tension increases, which is again in accordance with previous results (Figure 4). The second peak in Figure 6 is the agglomerate chord length distribution, this peak shifts to higher chord lengths when less Tween 20 is added. For the other curves, no mean particle size is calculated because it would be strongly influenced by the first peak of the droplets, resulting in too low values corresponding to the effective agglomerate size. The chord length corresponding to the maximum counts is used as the agglomerate size resulting in 160, 262, 364 and 504 µm for 0.50 x 10^{-3}, 0.79 x 10^{-3}, 1.03 x 10^{-3} and 1.40 x 10^{-3} N/m, respectively.

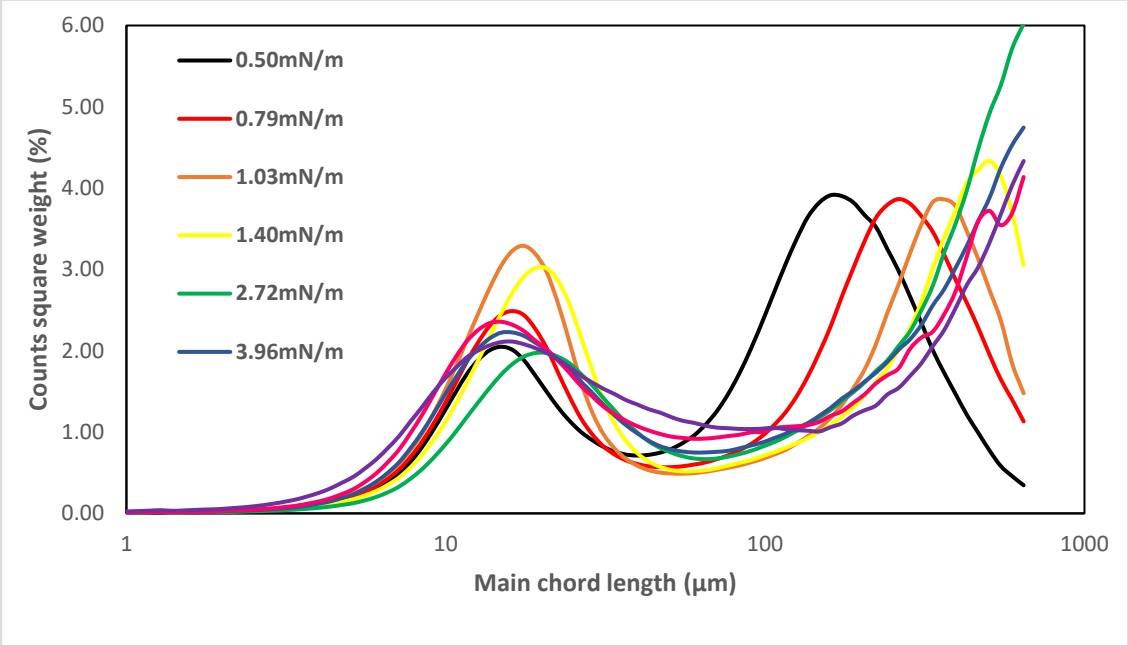

Figure 6: *Chord length distribution of the formed spherical agglomerates at varying interfacial tensions between BL and crystallization system.*

To obtain the particle sizes of the agglomerates larger than 700µm, offline measurements were performed after the filtration and drying steps. These results, together with the agglomerate sizes obtained from the Blaze probe, were plotted in function of the interfacial tension in Figure 7. To compare the offline measurement method with the inline sizing method, the agglomerates formed at an interfacial tension of 1.40 x 10^{-3} N/m were measured with both methods, as also shown in Figure 7. The offline measurement resulted in a larger agglomerate size of 709 µm in comparison with 504 µm for the Blaze measurements, which indicates that the agglomerate size should be interpreted with care. The difference is a result of the different methods and their outcomes, the Blaze probe gives the square weighted chord length, and the offline measurements result in volume based diameter. In case of the Blaze measurements, it is unclear which chord length was taken because only the data and raw images were given. For round particles, a difference between the chord length and the offline measurements is obtained, as the offline measurements always measure the effective diameter of the agglomerate, whereas the chord length measures the difference between two points on the edge of the circle and is only equal to the diameter of the circle if the points are in the exact opposite position on the circle. Thus,

it was expected that the chord lengths of spherical agglomerates would always be lower than the mean diameter obtained from the offline measurements. At the lowest interfacial tensions between 0.50 and 1.40 x 10^{-3} N/m, the agglomerate size increases linearly from 160 to 504 µm. In terms of Tween 20 concentration, the differences are rather large, ranging from 23.29 g/L to 4.63 g/L. The agglomerates with sizes between 1000 and 3500 µm were obtained by varying the Tween 20 concentration in toluene only from 0.095 to 1.62 g/L, which indicates very large differences in agglomerate sizes in comparison with the very small change in Tween 20 concentration. A blank spherical agglomeration experiment was performed without the addition of Tween 20 and thus with pure toluene as the bridging liquid, resulting in a mean particle size of 4412 µm at an interfacial tension of 37 x 10^{-3} N/m (Figure 7).

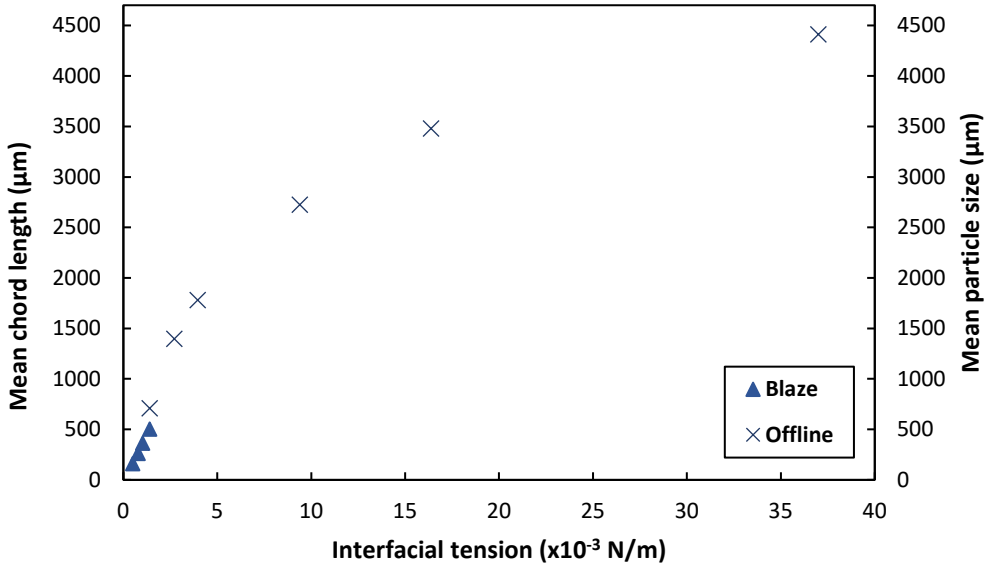

Figure 7: *The sizes of the obtained agglomerates plotted as a function of the interfacial tension. Blaze measurements result in mean square weighted chord lengths and the offline measurements in volume based mean particle size.*

Figures 8a-h shows the SEM images after the drying process of the formed agglomerates with increasing Tween 20 concentrations from a to h. Again, it is clearly shown how the agglomerate size decreases proportionally with the interfacial tension. The agglomerates shown in 8a and 8.b were even too large to fit on the image. Figure 8c-f clearly shows the decrease in agglomerate size and the spherical form of the agglomerates. The agglomerates of all concentrations are built up of needle- and plate-like benzoic acid crystals, which are comparable with the crystals formed when only the anti-solvent crystallization is performed, as shown in Figure 9. This indicates that the single crystals are insignificantly influenced by the agglomeration process, they were just packed together into the spherical agglomerates without changing. Figure 8a-h shows that the larger the agglomerates are, the smoother the edges of the agglomerates. A possible explanation is the larger ratio between agglomerate and single crystal size, which increases the probability that single crystals align completely with the surface of the agglomerates.

The agglomerates formed at interfacial tensions of 0.50 and 0.79 x 10^{-3} N/m started sticking together during the filtration process, resulting in the formation of a cake on the filter. This cake was also formed when only the anti-solvent crystallization was performed, and thus needle shaped crystals (Figure 9) were filtered, which results in bad filterability due to the shape. Figure 8h is a SEM image showing a part of the formed cake at 0.50 x 10^{-3} N/m in which no spherical agglomerates can be distinguished anymore.

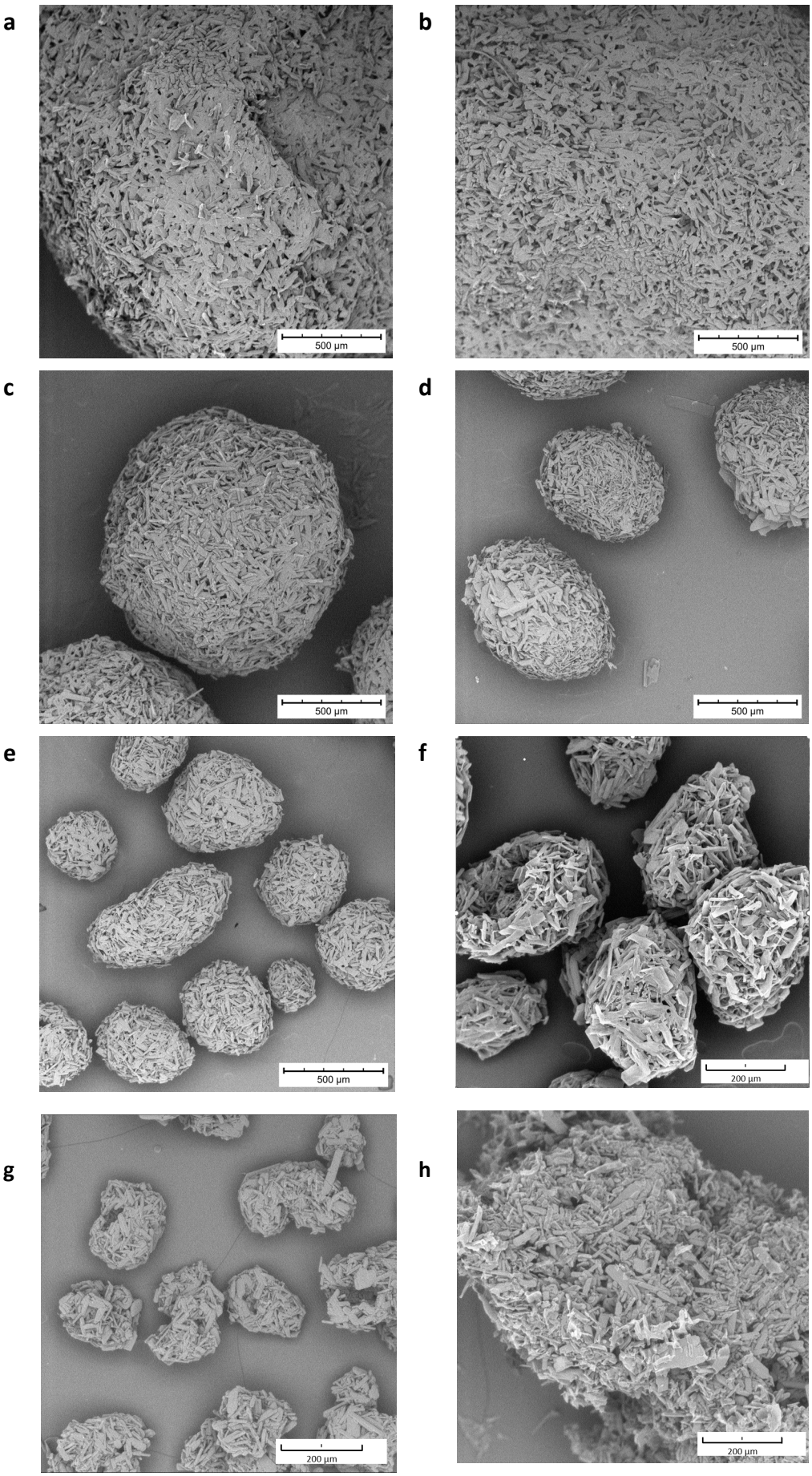
a
500 µm
b
500 µm
c
500 µm
d
500 µm
e
500 µm
f
200 µm
g
200 µm
h
200 µm

Figure 8: *SEM images of the obtained agglomerates after filtration and drying: a) 16.38 x 10^{-3} N/m, b) 9.39 x 10^{-3} N/m, c) 3.96 x 10^{-3} N/m, d) 2.72 x 10^{-3} N/m, e) 1.40 x 10^{-3} N/m, f) 1.03 x 10^{-3} N/m, g) 0.79 x 10^{-3} N/m, h) 0,50 x 10^{-3} N/m.)*

A possible explanation is an agglomerate breakup during the filtration, which corresponds to earlier findings in literature indicating that the agglomerate strength is proportional to the interfacial tension [6], [9]. The liquid bridges formed at 0.50 x 10^{-3} N/m are the weakest and probably not strong enough to overcome the forces applied by the vacuum filtration as agglomerates fall apart into needles and form a cake. However, it is remarkable that the agglomerates survived inside the reactor, in which a lot of shear is created due to the stirring speed of 1000 rpm. This might indicate that the crystals are bound by the liquid as long as the wet phase exists, but these bonds disappear during drying. Also, agglomerates formed at an interfacial tension of 0.79 x 10^{-3} N/m formed a cake during the filtration, but after carefully breaking it, some spherical shapes remained distinguishable, as shown in Figure 8g. The bad filterability in this case was probably a result of the bad alignment of the agglomerate edges, creating needle shapes at the agglomerate surface.

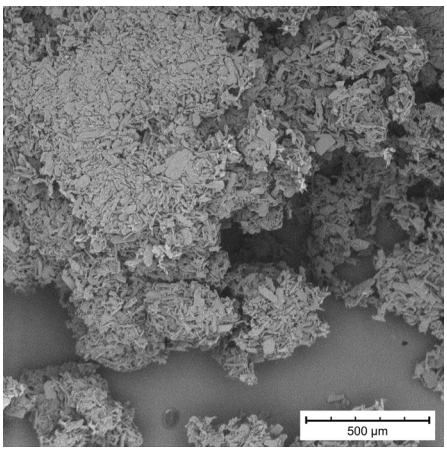

Figure 7: *SEM image of crystals obtained by anti-solvent crystallization.*

These results proved the ability to tune the size of spherical agglomerates by adding surfactants in varying concentrations. Particle sizes ranging from 160 µm up to 3481 µm were obtained by changing the surfactant concentration in the BL from 23.29 g/L to 0.095 g/L, respectively. When no surfactant was added, spherical agglomerates of 4412 µm were obtained, which indicates that even a very low amount of surfactant (0.095 g/L) decreases the agglomerate size by 1000 µm. At the highest concentrations (4.63 – 23.29 g/L) the agglomerate sizes are below 500 µm, resulting in a more precise tuneability of these small agglomerates due to the small differences in size in a large concentration range. At surfactant concentrations above 11.50 g/L, agglomerates formed inside the reactor fall apart during the vacuum filtration, indicating that the surfactant concentration in a real application should be determined carefully.

Finally, when comparing the change in agglomerate size to the change in BL droplet size at different times, as shown in Figure 4b a remarkable difference was noticed. The change in agglomerate size is more than 65 times higher than the change in BL droplet size. Based on this observation, it was hypothesized that the distribution mechanism occurs during the wetting step. Also, it seems that the agglomerate size is determined by coalescence during the agglomeration growth step, which is also confirmed by the fact that a lower surfactant concentration corresponds with a higher interfacial tension which causes more coalescence and thus larger agglomerates [4].

3.4 Residual toluene concentration

According to the European Medicine Agency, toluene belongs to the class 2 residual solvents in pharmaceuticals, which means that the residual concentration inside the medicine should be limited, but not avoided. Toluene has a low severe toxicity potential resulting in a limited permissible daily exposure

(PDE) of 8.9 mg/day, and an ICH residual solvent content limit of 890 ppm in drug substances. To evaluate the efficiency of the filtration and drying in terms of solvent removal, the residual toluene concentration inside the agglomerates is measured by GC-FID. The results are shown in Table 2 in which the interfacial tensions with their corresponding mean agglomerate sizes are listed with the residual toluene concentration. The overall trend shows an increase in residual toluene concentration with agglomerate size. This could be expected as an increased particle size corresponds with a decreased surface to volume area and thus slower solvent removal by diffusion and evaporation. During the filtration and drying, approximately the same mass of agglomerates was used, thus, the smaller agglomerates have a larger contact area, resulting in more efficient solvent removal. Also, the larger the particles, the more difficult it is to remove the solvent from the core of the particle due to the longer path of diffusion. For the smallest agglomerates, measured inline by the Blaze probe, the residual toluene concentration increases from 0.067 to 0.104 mg/g with a chord length increase from 160 to 505 µm. The larger agglomerates measured by the offline method show approximately the same trend, but the differences in toluene concentrations are smaller, ranging between 0.125 and 0.137 mg/g. The agglomerates with a mean particle size of 1396 µm resulted in a residual toluene concentration of 0.084 mg/g which is lower in comparison with the other agglomerates. In all cases, the residual toluene content remains well below the ICH limit of 0.89 mg/g.

Table 2: *Measured residual toluene concentrations in mg toluene / g sample for the agglomerates at varying interfacial tensions, listed with the mean agglomerate sizes. The blaze measurements show the mean chord length and the offline measurements show the mean diameter (D4,3). NA = not available*

Interfacial tension	**Agglomerate size (µm)**		**Residual toluene content**
(x10^{-3} N/m)	**Blaze**	**Offline**	**(mg/g)**
37.00	NA	4412	0.137
16.38	NA	3481	0.130
9.39	NA	2725	0.125
3.96	NA	1781	0.127
2.72	NA	1396	0.084
1.40	505	709	0.104
1.03	364	314	0.089
0.79	262	NA	0.109
0.50	160	NA	0.067

4 Conclusion

This study successfully demonstrated the capability of controlling the size of spherical agglomerates by adjusting the concentration of surfactant in the bridging liquid. It is hypothesized that this is attributed to the corresponding change in interfacial tension between BL and crystallization system. Initially, the study focused on investigating the impact of surfactant addition on the droplet size of the emulsion formed by the combination of the bridging liquid and crystallization solvent systems. The increase in droplet size was rather limited, ranging from 111 to 144 µm whereas the obtained spherical agglomerates sizes covered a broad range of agglomerate sizes from 160 to 3481 µm. This suggests that droplet size distribution may not be the decisive factor in spherical agglomeration processes. Instead, it is proposed that the coalescence of agglomerate nuclei is favored at higher surfactant concentration, leading to the formation of larger agglomerates. At the highest concentrations of Tween 20, the shape of the agglomerates became less aligned due to the smaller size ratio between single crystal and agglomerate. This irregular shape,

together with the decrease in agglomerate strength, is assumed to cause agglomerate collapse during vacuum filtration, resulting in cake formation. However, further research is necessary to extend these findings to other surfactants and confirm the obtained relationship between interfacial tension and agglomerate size.

Conflict of interest: The authors declare no conflict of interest.

Funding: Research foundation – Flanders (FWO) PhD Fellowship strategic basic research (1S68322N)

References

[1] S. Jitkar, R. Thipparaboina, R. B. Chavan, and N. R. Shastri, "Spherical Agglomeration of Platy Crystals: Curious Case of Etodolac," *Cryst. Growth Des.*, vol. 16, no. 7, pp. 4034–4042, 2016, doi: 10.1021/acs.cgd.6b00563.

[2] S. V. Patil and S. K. Sahoo, "Spherical Crystallization : a Method to Improve Tabletability," *Res. J. Pharm. Technol.*, vol. 2, no. 2, pp. 234–237, 2009.

[3] Y. Kawashima and M. Imai, "Development of agglomerated crystals of Ascorbic acid by the spherical crystallization technique for direct tableting and evaluation of their comactibilities," *KONA Powder Part. J.*, vol. 168, no. 20, pp. 160–168, 2002.

[4] J. Thati, "Particle Engineering by Spherical Crystallization:Mechanisms and Influence of Process Conditions," Royal institute of Technology, 2011.

[5] P. M. Orlewski, B. Ahn, and M. Mazzotti, "Tuning the particle sizes in spherical agglomeration," *Cryst. Growth Des.*, vol. 18, no. 10, pp. 6257–6265, 2018, doi: 10.1021/acs.cgd.8b01134.

[6] B. Kovačič, F. Vrečer, and O. Planinšek, "Spherical crystallization of drugs," *Acta Pharm.*, vol. 62, no. 1, pp. 1–14, 2012, doi: 10.2478/v10007-012-0010-5.

[7] A. Nitsure, D. Patel, and S. Wairkar, "Improved processability of ethambutol hydrochloride by spherical agglomeration," *Pharm. Dev. Technol.*, vol. 25, no. 3, pp. 376–384, 2020, doi: 10.1080/10837450.2019.1705487.

[8] K. Tahara, Y. Kono, A. S. Myerson, and H. Takeuchi, "Development of Continuous Spherical Crystallization to Prepare Fenofibrate Agglomerates with Impurity Complexation Using Mixed-Suspension, Mixed-Product Removal Crystallizer," *Cryst. Growth Des.*, vol. 18, no. 11, pp. 6448–6454, 2018, doi: 10.1021/acs.cgd.8b00426.

[9] J. Thati and Å. C. Rasmuson, "Particle engineering of benzoic acid by spherical agglomeration," *Eur. J. Pharm. Sci.*, vol. 45, no. 5, pp. 657–667, 2012, doi: 10.1016/j.ejps.2012.01.006.

[10] R. Peña, D. J. Jarmer, C. L. Burcham, and Z. K. Nagy, "Further Understanding of Agglomeration Mechanisms in Spherical Crystallization Systems : Benzoic Acid Case Study," *Cryst. Growth Des.*, vol. 19, pp. 1668–1679, 2019, doi: 10.1021/acs.cgd.8b01519.

[11] J. Katta and Å. C. Rasmuson, "Spherical crystallization of benzoic acid," *Int. J. Pharm.*, vol. 348, pp. 61–69, 2008, doi: 10.1016/j.ijpharm.2007.07.006.

[12] D. Amaro-Gonzalez and B. Biscans, "Spherical agglomeration during crystallization of an active pharmaceutical ingredient," *Powder Technol.*, vol. 128, pp. 188–194, 2002.

[13] C. Subero-couroyer, D. Mangin, A. Rivoire, A. F. Blandin, and J. P. Klein, "Agglomeration in suspension of salicylic acid fine particles : Analysis of the wetting period and effect of the binder injection mode on the final agglomerate size," *Powder Technol.*, vol. 161, pp. 98–109, 2006, doi: 10.1016/j.powtec.2005.08.014.

[14] C. Yu *et al.*, "Design of the spherical agglomerate size in crystallization by developing a two-step bridging mechanism and the model," *AIChE J.*, vol. 68, no. 2, pp. 1–18, 2022, doi: 10.1002/aic.17526.

[15] S. Guo *et al.*, "Design of spherical agglomerates via crystallization with a non-toxic bridging liquid: From mechanism to application," *Powder Technol.*, vol. 408, no. June, p. 117725, 2022, doi: 10.1016/j.powtec.2022.117725.

[16] J. Thati and Å. C. Rasmuson, "On the mechanisms of formation of spherical agglomerates," *Eur. J. Pharm. Sci.*, vol. 42, no. 4, pp. 365–379, 2011, doi: 10.1016/j.ejps.2011.01.001.

[17] K. Pitt *et al.*, "Particle design via spherical agglomeration: A critical review of controlling parameters, rate processes and modelling," *Powder Technol.*, vol. 326, pp. 327–343, 2018, doi: 10.1016/j.powtec.2017.11.052.

[18] M. Maghsoodi, "Effect of process variables on physicomechanical properties of the agglomerates obtained by spherical crystallization technique," *Pharm. Dev. Technol.*, vol. 16, no. 5, pp. 474–482, 2011, doi: 10.3109/10837450.2010.492218.

[19] Y. Kawashima, M. Okumura, and H. Takenaka, "The Effects of Temperature on the Spherical Crystallization of Salicylic acid," *Powder Technol.*, vol. 39, pp. 41–47, 1984.

[20] A. F. Blandin, D. Mangin, A. Rivoire, J. P. Klein, and J. M. Bossoutrot, "Agglomeration in suspension of salicylic acid fine

particles : influence of some process parameters on kinetics and agglomerate final size," *Powder Technol.*, vol. 130, pp. 316–323, 2003.

[21] R. Peña and Z. K. Nagy, "Process Intensification through Continuous Spherical Crystallization Using a Two-Stage Mixed Suspension Mixed Product Removal (MSMPR) System," *Cryst. Growth Des.*, vol. 15, no. 9, pp. 4225–4236, 2015, doi: 10.1021/acs.cgd.5b00479.

[22] R. Pena, J. A. Oliva, C. L. Burcham, D. J. Jarmer, and Z. K. Nagy, "Process Intensification through Continuous Spherical Crystallization Using an Oscillatory Flow Baffled Crystallizer," *Cryst. Growth Des.*, vol. 17, no. 9, pp. 4776–4784, 2017, doi: 10.1021/acs.cgd.7b00731.

[23] A. Vancleef, D. Maes, T. Van Gerven, L. C. J. Thomassen, and L. Braeken, "Flow-through microscopy and image analysis for crystallization processes," *Chem. Eng. Sci.*, vol. 248, p. 117067, 2021, doi: 10.1016/j.ces.2021.117067.

[24] A. Bąk and W. Podgórska, "Interfacial and surface tensions of toluene/water and air/water systems with nonionic surfactants Tween 20 and Tween 80," *Colloids Surfaces A Physicochem. Eng. Asp.*, vol. 504, pp. 414–425, 2016, doi: 10.1016/j.colsurfa.2016.05.091.